Repository Istituzionale dei Prodotti della Ricerca del Politecnico di Bari

High-Q Spiral Resonator for Optical Gyroscope Applications: Numerical and Experimental Investigation

This is a post print of the following article

Original Citation:
High-Q Spiral Resonator for Optical Gyroscope Applications: Numerical and Experimental Investigation / Ciminelli, Caterina; Dell'Olio, Francesco; Armenise, Mario Nicola. - In: IEEE PHOTONICS JOURNAL. - ISSN 1943-0655. - 4:5(2012), pp. 1844-1854. [10.1109/JPHOT.2012.2218098]

Availability:
This version is available at http://hdl.handle.net/11589/3580 since: 2016-11-04

Published version
DOI:10.1109/JPHOT.2012.2218098

Publisher:

Terms of use:

(Article begins on next page)

02 May 2026

IEEE Photonics Journal
An IEEE Photonics Society Publication

Open Access

High-Q Spiral Resonator for Optical Gyroscope Applications: Numerical and Experimental Investigation

Volume 4, Number 5, October 2012

Caterina Ciminelli
Francesco Dell'Olio
Mario N. Armenise

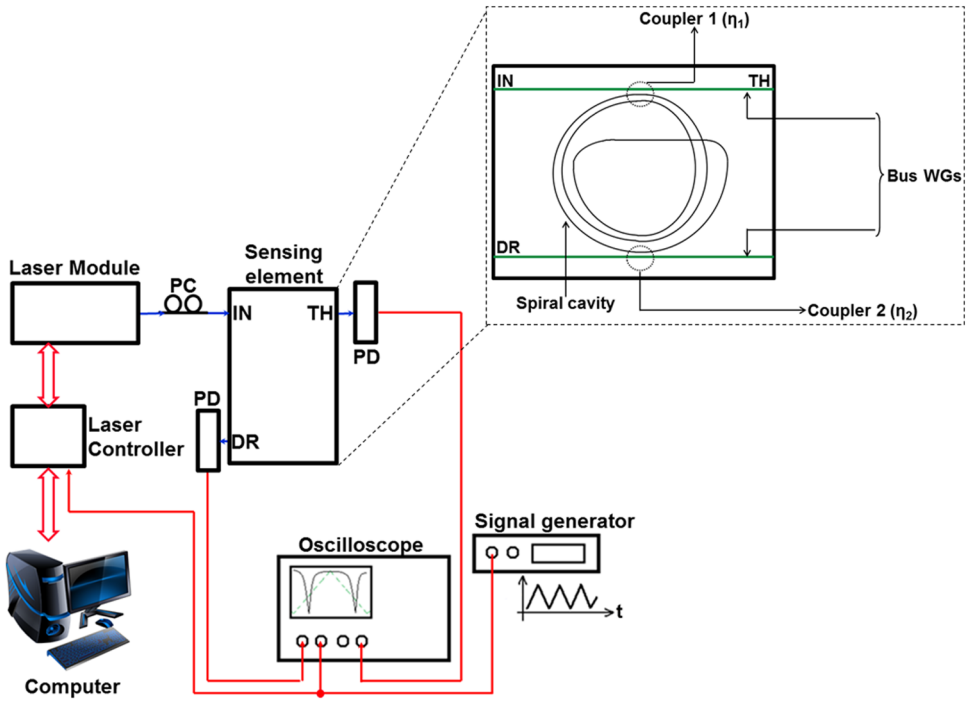

DOI: 10.1109/JPHOT.2012.2218098
1943-0655/$31.00 ©2012 IEEE

IEEE photonics SOCIETY

IEEE

High-Q Spiral Resonator for Optical Gyroscope Applications: Numerical and Experimental Investigation

Caterina Ciminelli, Francesco Dell'Olio, and Mario N. Armenise

Optoelectronics Laboratory, Politecnico di Bari, 70125 Bari, Italy

DOI: 10.1109/JPHOT.2012.2218098
1943-0655/$31.00 ©2012 IEEE

Manuscript received July 27, 2012; revised August 30, 2012; accepted September 5, 2012. Date of publication September 10, 2012; date of current version September 24, 2012. This work was supported by the European Space Agency under MiOS Project 4000102311/10/NL/PA. Corresponding author: C. Ciminelli (e-mail: c.ciminelli@poliba.it).

Abstract: This paper reports the numerical and experimental results of a high-Q silica-on-silicon spiral resonator to be used in microoptical gyroscopes having a potential resolution $< 10\ ^\circ$/h. First, demonstration of a Ge:SiO_2 waveguiding spiral cavity as sensing element for gyro applications is given, and results of its optical characterization are provided. Quality factor, finesse, free spectral range, and thermal stability have been measured, clearly showing the potential of the device for gyro applications. The effect of coupling tuning through micrometer scale heaters and the supported eigenstates of polarization have also been experimentally investigated. The thermal stabilization of the silica chip is realized using a thermoelectric cooler co-packaged with the resonant cavity. The Q-factor of the spiral exceeds 10^6, and the thermal drift of the resonance frequency is very low (< 20 kHz/s). An original formula estimating the bias drift due to the Kerr effect has been derived, proving that a bias drift of 0.2 $^\circ$/h can be achieved by controlling the polarization noise. The resolution of the angular velocity sensor has been numerically estimated by exploiting the experimental results. We demonstrate that the resolution of our device can be improved to values less than 10 $^\circ$/h, by decreasing both the propagation loss within the resonator (< 0.05 dB/cm, which is currently achievable) and the cavity insertion loss to 1–2 dB (typical value).

Index Terms: Integrated optics, optical resonators, gyroscopes.

1. Introduction

In the last few years, miniaturization of both mechanical and optical gyroscopes has been identified as a crucial research target because the high-performance angular velocity sensors currently available on the market often do not fully meet the requirements in terms of weight, volume, and power consumption of several emerging applications (e.g., inertial navigation of micro- and nanosatellites) [1].

Silicon-based MEMS angular velocity sensors [2], which are compact mechanical gyroscopes based on the Coriolis effect, are commercially available devices and have a constantly growing market.

Unfortunately, with a resolution $> 100\ ^\circ$/h, they have not yet reached the performance requested by inertial navigation systems (INSs; $< 10\ ^\circ$/h) and some reliability issues still remain.

Optical gyroscopes [3] based on either semiconductor ring lasers (SRLs) or passive cavities were first proposed about four decades ago [4], [5]. Currently, they are the topic of intense research effort aimed at the development of a new generation of optical gyros having reliability, resolution, and bias

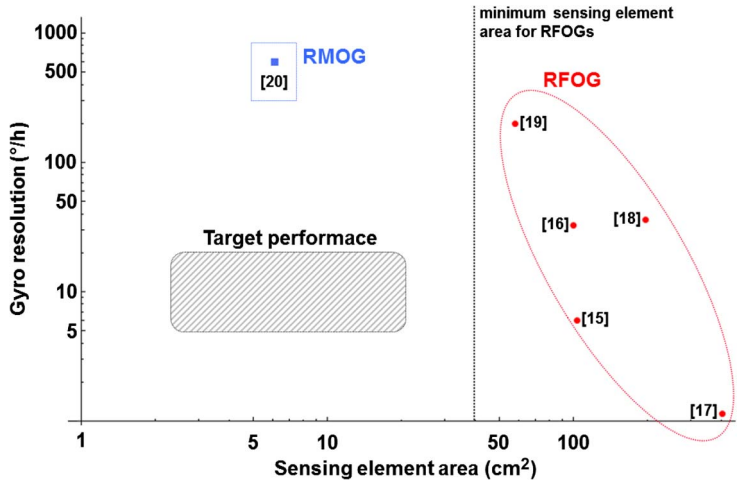

Fig. 1. State of the art of the resonant optical gyroscopes. For comparison, integration time = 1 s has been assumed for all sensors. Only experimentally measured resolution values were considered. Log scale has been used for both axes.

stability compatible with inertial navigation applications while being more compact and having lower power consumption than conventional optical gyros (He–Ne ring laser gyroscope and interferometric fiber optic gyroscope), which currently cover a wide performance range (resolution from 0.01 to 10 °/h).

SRL-based gyros [6]–[9] have a very small area (footprint < 1 cm^2) and low power consumption. However, they suffer from backscattering and mode competition within the active semiconductor cavity and require a significant dithering to operate.

Optical angular velocity sensors based on a single passive resonator [10], which are considered ideal candidates for optoelectronic gyro scaling, exploit the resonance frequency shift suffered from a rotating optical cavity (sensing element). The resonator quality factor Q has to be maximized because it strongly affects the resolution of these devices. Therefore, large-area cavities with high Q-values ($Q > 10^5$) realized using either optical fibers [11] or low-loss integrated optical technologies (e.g., glass or silica-on-silicon) [12], [13] are usually key components of these sensors. Resonators with a loss compensation mechanism such as the integration of an amplifying section along the optical path have also been proposed in this context [14].

Resonant fiber-optic gyroscopes (RFOGs) perform very well (resolution less than a few tens of °/h [15]–[18]), but unfortunately, they cannot be miniaturized because the size of their sensing element has to be > 40 cm^2 to avoid too high bending loss in the fiber resonator. In [19], an RFOG including the most compact sensing element available to our knowledge (an air-core fiber resonator occupying an area > 50 cm^2) shows a resolution of 200 °/h, assuming the sensor bandwidth = 1 s.

Integrated gyros based on planar passive cavities [also called resonant microoptical gyros (RMOGs)] have recently reached good compactness and interesting values of minimum detectable angular velocity (several hundreds of °/h with a sensing element footprint = 6.3 cm^2 [20]). In any case, further improvements are needed to achieve the resolution range 1–10 °/h that is required by new key application domains (e.g., planetary rovers) and currently uncovered by silicon MEMS gyros.

The state of the art of resonant optical gyros (RFOGs and RMOGs) is summarized in Fig. 1. RMOGs are still far from the 1–10 °/h resolution range, while RFOGs are not able to scale to the level demanded by current miniaturization trends. RMOG prototypes proposed in the literature include packaged optoelectronics components in different technologies that are connected by optical fibers. Hybrid integration of these components, for example by silicon optical bench (SiOB) technology, is an engineering activity with a few critical aspects that may allow the realization of a

single-axis gyro with a volume less than 30 cm^3. A volume that seems to be hardly achievable using RFOG technology.

In this paper, we report on the optical characterization of a high-Q silica-on-silicon resonator having a spiral configuration with a length of 42 cm and a footprint of 20 cm^2. The aim of our paper was the design and fabrication of an RMOG with a sensing element area < 20 cm^2 and a resolution close to 10 °/h.

To our knowledge, the characterized device is the first experimental demonstration of a spiral cavity for angular velocity sensing.

On the basis of the experimental results, we discuss the potential performance of the RMOG based on the spiral cavity by also introducing an original expression of the bias drift induced by the Kerr effect.

Preliminary results of the optical characterization was reported and briefly discussed in [21], where only the cavity spectral response was shown. In this paper, additional important features of the resonator are provided, together with details on how to experimentally build the spectral response of the sensor and a complete numerical prediction of the gyro performance.

2. Experimental Characterization of the Resonator

The integrated optical resonator used has a three-loop spiral configuration, which was selected to increase the optical path of the resonant modes within the cavity, avoiding a too large footprint.

The manufactured spiral, which was modeled and designed in [22] and [23], is 42 cm long, and was made using a single-mode 6 μm $\times$ 6 μm Ge-doped silica waveguide (effective index $= 1.457$). The index contrast between the Ge-doped silica and the undoped silica surrounding the core is 0.75%. Flame hydrolysis deposition (FHD) technology was exploited for the device fabrication.

The value of spiral length has been chosen after an accurate optimization achieved through a complete physical model of the angular velocity sensor [24].

The standard deviation of sidewall roughness in the silica waveguide was about 200 nm. Experimentally measured propagation loss of the guiding structure was equal to 0.1 dB/cm [23] for the TE polarization. The agreement between that value and the loss numerically predicted in [25] is very good.

The two crossing points in the spiral (see the sensing element configuration in Fig. 2) were designed with an angle close to 90° in order to make their optical losses < 0.01 dB.

The cavity is evanescently coupled to two straight bus waveguides and the coupling ratio between these waveguides and the resonator can be thermally tuned by two heaters placed near the couplers. The bus waveguides are butt coupled to single-mode polarization maintaining fiber pigtails. The resonator is thermally stabilized by a thermoelectric cooler (TEC).

The characterization setup for the estimation of the resonator spectral response (see Fig. 2) has been already described in [21]. It includes a thermally stabilized laser module operating at 1.55 μm, the laser controller, two Ge photodetectors, a fiber polarization controller, a signal generator, an oscilloscope, and a TEC controller.

The laser emission frequency (linewidth $<$ 10 kHz) can be tuned through either piezoelectric tuning (in the 300-MHz range) or thermal tuning (in the 30 000-MHz range). The piezoelectric tuning is linear and fast (modulation speed up to 30 kHz), whereas the thermal tuning is slow.

To evaluate the spectral response, the sensing element is excited by the laser source whose emission frequency is linearly tuned in a 300-MHz range by applying to the laser controller a triangular waveform generated by the signal generator. The laser scans a 300-MHz section of the resonator spectral response, as shown in Fig. 3(a). Since the cavity free spectral range (FSR) is 500 MHz, the scanned section only includes a portion of the spectral response. Therefore, several acquisitions of the oscilloscope waveforms are needed to reconstruct the whole spectral response. These acquisitions are performed for different values of the laser central frequency, which can be thermally tuned within the 30 000-MHz range [see Fig. 3(b)].

Normalized spectral responses of the silica-on-silicon cavity at both the through and drop port were reported in [21] and are shown in Fig. 4 as the result of the laser scanning illustrated in Fig. 3.

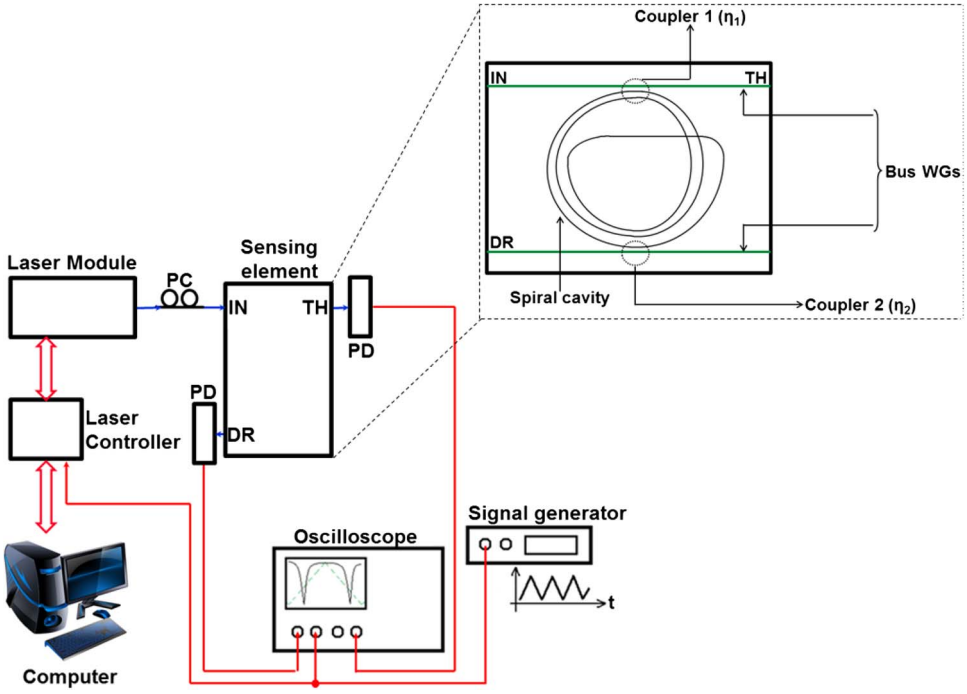

Fig. 2. Sensing element configuration. WG: waveguide. η_1 and η_2 are the coupling ratios IN: input port. TH: through port. DR: drop port. The sensing element is shown in the inset.

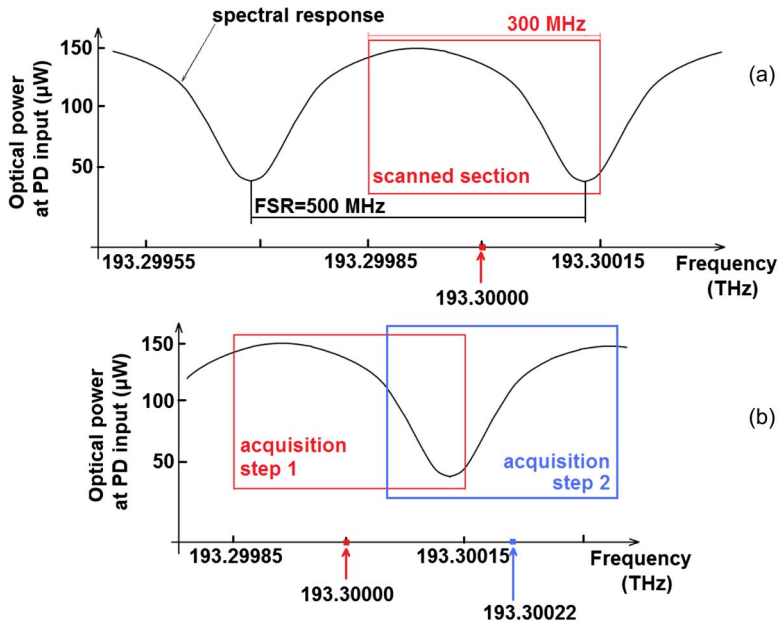

Fig. 3. (a) Portion (in red) of the spectral response of the cavity scanned by the laser through acquisition step 1. Laser central frequency = 193.30000 THz. (b) Spectrum regions relevant to acquisition steps 1 and 2. Laser central frequency for the second acquisition step is 193.30022 THz.

A significant value of the resonance depth at the through and drop port was obtained. Measured values of full width at half-maximum and FSR allowed to calculate the quality factor Q as high as 1.5×10^6 and the finesse $F = 4.2$.

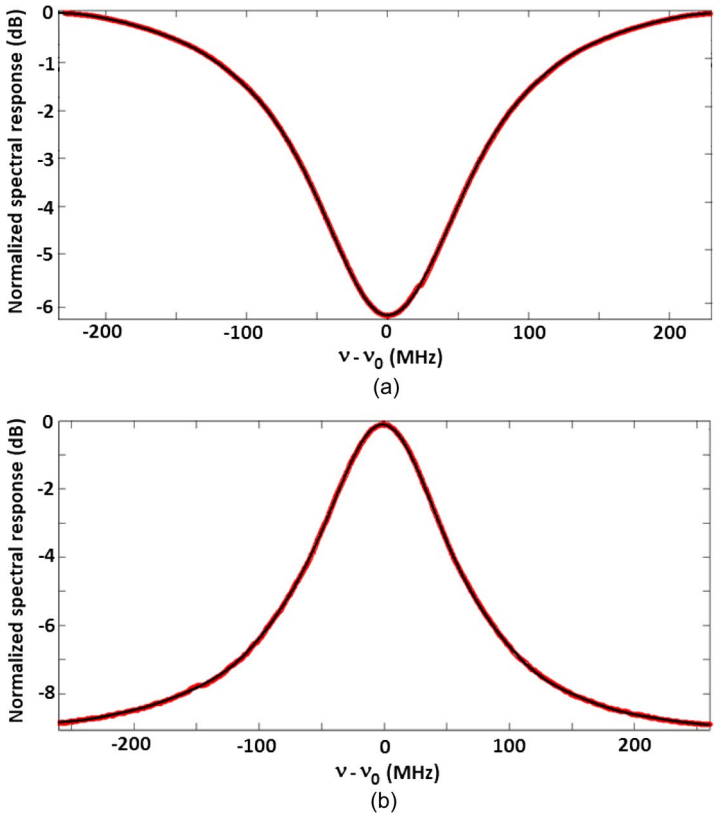

Fig. 4. Resonator spectral response at through (a) and drop port (b). Resonance frequency: ν_0. Frequency: ν.

TABLE 1

Coupler parameters estimated on the basis of the experimental measurements

Parameter	Estimated value
Coupler 1 coupling ratio (η_1)	36%
Coupler 1 loss	3%
Coupler 2 coupling ratio (η_2)	17 %
Coupler 2 loss	7 %

Using the measured spectra, the coupling ratios η_1 and η_2 and coupler loss have been estimated by a nonlinear curve-fitting technique (see Table 1). These values were calculated with the coupler tuning control switched off. The coupling ratio values are very close to the designed ones, which were selected to optimize the quality factor while keeping the resonance depth $>$ 6 dB.

A chip temperature change induces a drift of the resonance frequency. We first measured the thermal drift of the resonance frequency without connecting the sensing element to the TEC controller. Without any thermal stabilization, the resonance frequency drift is about 200 $\div$ 400 kHz/s. When the TEC controller is switched on and connected to the Peltier cell co-packaged with the silica chip, the drift decreases to 20 kHz/s.

The thermal drift was measured in our laboratory, where the temperature was about 25 °C $\pm$ 1 °C over a few hours. The TEC controller has a resolution of 0.01 °C, an accuracy of $\pm$0.1 °C, and

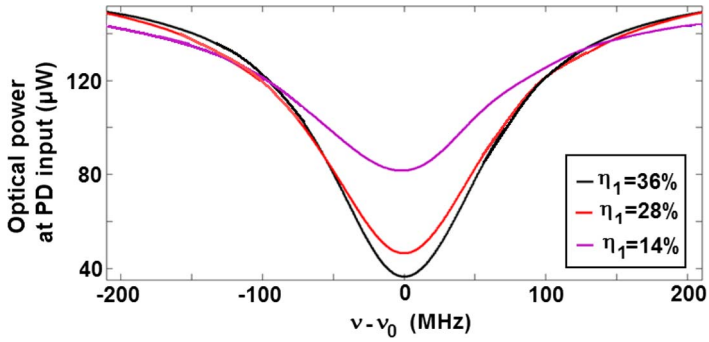

Fig. 5. Resonator spectral response at the through port when the coupling ratio η_1 is tuned in the range $14 \div 36\%$.

TABLE 2

Resonator performance (relevant to the through response) for several values of the current Injected in Heater 1

Parameter	i = 0 mA	i = 150 mA	i = 200 mA
Resonance depth	6.2 dB	5.1 dB	2.5 dB
FWHM (MHz)	121	136	160
Quality factor	1.5×10^6	1.4×10^6	1.2×10^6
Coupler 1 coupling ratio	36%	28%	14%
Coupler 1 loss	3%	27%	58%

a temperature stability over 24 hours of $< 0.002\ ^\circ$C. The warm-up time for maximum accuracy is $<$ 10 min.

The coupling ratio of both couplers were tuned with two heaters, observing that the current injected in the heaters decreases the coupling ratio and increases the coupler loss.

The coupling ratio η_1 was thermally tuned in the range $14 \div 36\%$ and η_2 kept constant at 17%. The through spectral response was observed for three different values of η_1 (see Fig. 5).

Due to the increase in the coupler loss, the tuning induces a linewidth widening and consequently a *Q*-factor decrease. The resonance depth also decreases. Table 2 summarizes the cavity performance measured when η_1 is changed by injecting the current *I* in heater 1 to control coupler 1.

As in the case of the η_1 variation, the tuning of η_2, keeping η_1 constant, and the tuning of both coupling ratios cause both a degradation of the sensing element performance in terms of *Q*-factor and resonance depth, and a decrease in the resonance thermal stability.

As demonstrated in [26], two eigenstates of polarization (ESOPs) can be excited in the resonator. Since the waveguide index contrast is low $(= 0.75\%)$ and the spiral bending radius is large (> 2 cm), the coupling between the two ESOPs and, in turn, the polarization conversion within the cavity can be neglected. As in the case of the fiber ring resonator, the two ESOPs of the silica cavity can be considered as orthogonal.

The two ESOPs resonate at different frequencies and the difference between them is proportional to the waveguide birefringence (difference between the effective indices of the quasi-TE and quasi-TM modes). Since the waveguide has a birefringence of about 7×10^{-7}, the difference between the resonances of the two ESOPs is about 100 MHz.

The polarization controller included in the characterization setup allows either one or both the ESOPs to be excited (see Fig. 6). The excitation of just one ESOP implies that the state of polarization (SOP) of the input beam is matched to the excited ESOP. This matching condition can

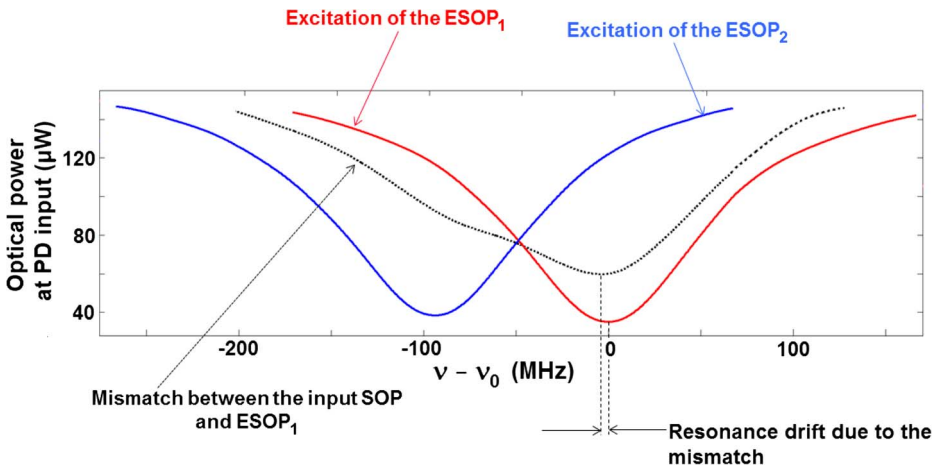

Fig. 6. Resonator spectral response at the through port in three operating conditions, i.e., the input SOP is matched with the $ESOP_1$, the input SOP is matched with the $ESOP_2$, the input SOP is not fully matched with the $ESOP_1$.

be achieved by regulating the PC. The mismatch between the input SOP and the excited ESOP induces a drift of the resonance frequency and a change of the spectral response shape (in particular, the resonance depth decreases), as clearly shown in Fig. 6.

3. Gyro Performance Discussion

Data provided by the experimental characterization of the sensing element, namely, the spiral cavity, allow the estimation of the two key performance parameters of our sensor prototype, i.e., the sensor resolution (or minimum detectable angular velocity) and the bias drift.

Our sensor has a closed-loop configuration and the readout system is based on phase modulation spectroscopy. Key prototype components are the laser and the PDs already included in the characterization setup (see Fig. 2), two phase modulators and two acousto-optic frequency modulators (AOMs) for processing both optical beams coming out of a beam splitter placed at the laser output, and an electronic module with a two channel lock-in amplifier and a digital section implementing the readout algorithm.

The two beams coupled in the cavity excite two counterpropagating resonant modes having the same resonance order. Resonant frequencies of these modes are split by rotation, and according to the Sagnac effect, the difference between them $(\Delta\nu)$ is proportional to the angular rate Ω applied to the cavity. The measurement of this difference, which yields the angular velocity, is carried out by the readout optoelectronic circuit that includes the electronic module, photodiodes, and modulators.

Since the average optical power at the input of the photodiodes P_{pd}, is typically in the range of μW or mW, we assume that the resolution is shot noise limited.

The shot-noise-limited resolution $\delta\Omega$ of frequency-sensitive gyros based on a passive cavity is given by [26]

$$\delta\Omega = \frac{\nu_S\sqrt{2}}{Q \cdot S}\Pi \tag{1}$$

where

$$\Pi = \sqrt{Bh\nu_S/\eta_{pd}P_{pd}} \tag{2}$$

ν_S is the sensor operating frequency (= 193 THz, corresponding to an operating wavelength of 1.55 μm), S is the gyro scale factor in terms of $\Delta\nu/\Omega$, B is the sensor bandwidth, h is Planck's constant, and η_{pd} is the quantum efficiency of the two photodiodes.

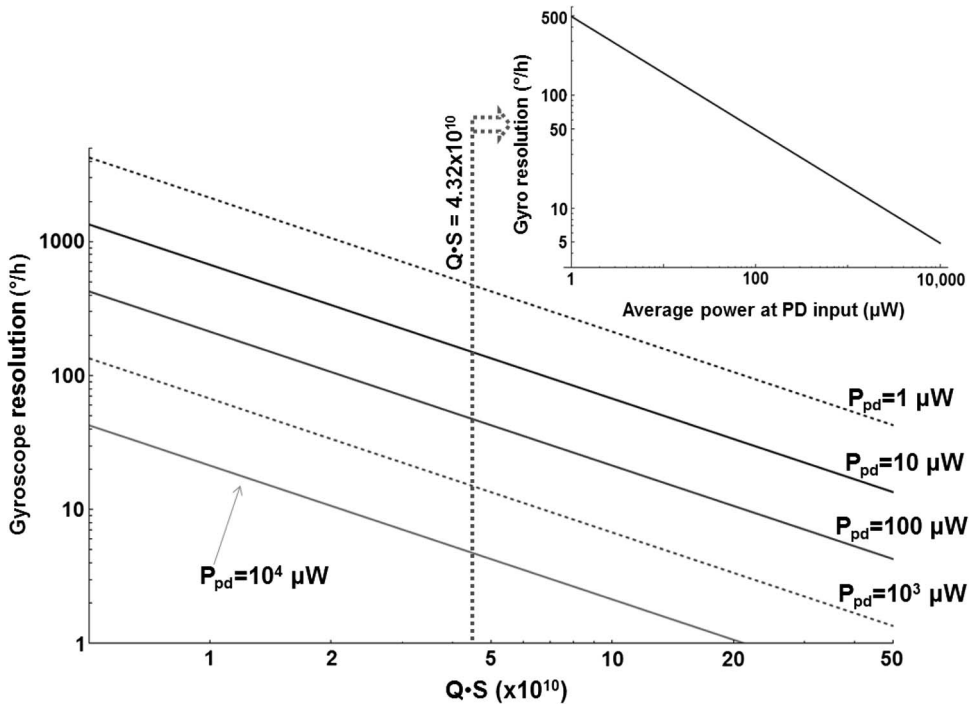

Fig. 7. Gyro resolution dependence on the $Q \cdot S$ product for several values of P_{pd}. In the inset, the $\delta\Omega$ dependence on P_{pd} for $Q \cdot S = 4.32 \times 10^{10}$ is shown.

The two fundamental parameters influencing $\delta\Omega$ are the product $Q \cdot S$ and the average power at the input of the photodiodes. The quality factor mainly depends on the propagation loss within the optical cavity, whereas S can be enhanced only by increasing the resonator footprint (we assume that the sensor operating wavelength is constant). The average power at the photodiode inputs depends on both the laser power and the total loss suffered from the optical beam along its path from the laser to the photodetectors.

In Fig. 7, the resolution dependence on the $Q \cdot S$ product for four P_{pd} values is shown. Log scale has been used for both axes. We assume $B = 1$ Hz and $\eta_{pd} = 0.9$. The resolution decreases when $Q \cdot S$ increases, for all P_{pd} values. For a specific value of $Q \cdot S$, $\delta\Omega$ decreases when P_{pd} increases. Since an improvement of $\delta\Omega$ can be achieved by increasing either the product $Q \cdot S$ or the average power at the photodiodes, the four strategies listed in Table 3 can be used for resolution enhancement. Limitations imposed by technological constraints and/or potential critical aspects are highlighted for each approach.

As reported in [21], we obtained $Q \cdot S = 4.32 \times 10^{10}$ ($Q = 1.5 \times 10^6$ and $S = 2.88 \times 10^4$) and the measured $P_{pd} = 10$ μW, which is quite low also because of nonoptimized fiber/waveguide coupling. The shot-noise-limited gyro resolution, estimated by (1), is equal to 156 °/h. This value is about 7% better than the value theoretically estimated for the prototype reported in [20].

To improve the value of the figure of merit $Q \cdot S$ without enlarging the sensor footprint, a higher value of Q is required. This can be achieved by optimizing the resonator fabrication process to decrease the propagation loss below 0.1 dB/cm. Since the sensing element footprint is already large (about 20 cm^2), an improvement of $Q \cdot S$ can be only achieved by increasing Q. This can be done. For example, if the propagation loss is halved, the quality factor increases by about 20%. In this case, the target performance $\delta\Omega = 10$ °/h is achieved for $P_{pd} = 1$ mW.

From Fig. 7, it can be observed that, for $Q \cdot S = 4.32 \times 10^{10}$ and $P_{pd} = 2.4$ mW $(= 3.8$ dBm$)$, we obtain $\delta\Omega = 10$ °/h. This P_{pd} value can be achieved if the total loss suffered from the optical beam along the whole optical path is equal to 13.6 dB, which is fully compliant with both the performance

TABLE 3

Strategies for resolution enhancement

Parameter	Increase/ Decrease (↑/↓)	Limitations and/or critical aspects
Laser power	↑	High-power and narrow-linewidth lasers are typically very expensive.
Propagation loss within the resonator	↓	It is very difficult to reduce propagation loss below 0.01 dB/cm.
Optical beam loss in its path from the laser to the photodetector	↓	Due to the number of components that the beam passes through from the laser to the photodetector, reasonable values of this parameter are ≥ 10 dB.
Resonator footprint	↑	The consequence of a too large footprint could be a non-uniform fabrication process.

of market-available components forming the prototype and the state of the art of silica-on-silicon technology.

The gyro bias drift is due to two contributions, i.e., polarization noise and the Kerr effect. The contribution due to backscattering is negligible because the sensing element is excited by two beams at different frequencies (the prototype includes two independent AOMs), and thus, the counterpropagating resonant modes excited within the cavity are decoupled.

For each beam exciting the cavity, the condition of full matching between the input SOP and one of the two ESOPs has to be fulfilled. The input SOPs and/or the ESOP to be excited change with mechanical vibrations and/or thermal fluctuations, and this can perturb the matching condition, inducing in turn a resonance drift and, thus, contributing to the gyro bias drift.

Due to fabrication tolerances, the optical intensities (I_1 and I_2) of the two cavity resonant modes may be different. Because of the Kerr effect, the difference ΔI between the intensities induces a bias in the gyro output, which is given by the following expression, derived in the Appendix:

$$\Delta\Omega = \frac{\nu_0}{2n_{\text{eff}}^2}\frac{n_2}{A_{\text{eff}}}\frac{1}{S}\Delta I \tag{3}$$

where A_{eff} is the waveguide effective area (about 40 μm^2), and n_2 is the waveguide nonlinear-index coefficient $(= 2.6 \times 10^{-20}$ m^2/W$)$. The drift of ΔI, which is due to the drift of the beam splitter and the two couplers realized on the silica chip, contributes to the gyro bias drift. Equation (3) shows that $\Delta\Omega$ is inversely proportional to the sensor scale factor. This means that a scale factor increase induces a reduction of the bias drift due to the Kerr effect. The increase of the scale factor implies the increase of the resonator footprint, which we assumed not exceeding a few tens of cm^2. Thus, reasonable values of S are less than 5×10^4.

In our prototype, the main contribution to the bias drift is due to the Kerr effect. In fact, we verified that the mismatch between the input SOPs and the cavity ESOPs is always $< 0.5^\circ$, and thus, using the mathematical model reported in [26], we can conclude that the bias drift due to polarization noise is $\ll 1$ °/h.

The intensities of the two resonant modes are approximately equal to 100 μW, and the drift of I_1 and I_2 is equal to 1%. Thus, the drift of both I_1 and I_2 is 1 μW (1% of 100 μW), resulting in $\Delta I = 2$ μW, which induces a gyro bias drift of 0.2 °/h.

The drift of I_1 and I_2 could be reduced to 0.5% by substituting the fiber beam splitter currently used with another one realized using silica-based planar lightwave circuit technology. In this case, the bias drift induced by the Kerr effect should be about 0.1 °/h. Recently [19], a gyro based on an air-core fiber has been proposed to reduce the Kerr-induced drift and thermal polarization instability.

4. Conclusion

Both experimental results on the first high-Q spiral resonator for angular velocity sensing and calculated performance of the RMOG including that resonator are presented in this paper.

Optical characterization of the sensing element is reported and discussed, together with the evaluation of the cavity performance and how to improve it. The quality factor is 1.5×10^6, the finesse is 4.2, and the resonance thermal drift is reduced down to 20 kHz/s, after thermally stabilizing the silica chip. The resonator supports two orthogonal ESOPs resonating at two frequencies that exhibit a difference of 100 MHz, which means that the waveguide birefringence is of the order of 10^{-7}. The effect of mismatch between the input SOP and the two eigenstates on the resonance frequency has been demonstrated.

The gyroscope resolution was calculated by assuming that it is limited by the shot noise.

An original formula has been derived to predict the Kerr-effect bias drift, and the key physical parameters influencing that noise source have been identified. We have theoretically proved that a bias drift of about 0.2 °/h can be achieved after implementing appropriate technological solutions for polarization noise mitigation.

To our knowledge, we have demonstrated for the first time, on the basis of both theoretical and experimental results, the possibility of realizing an RMOG, including a spiral waveguiding resonator, with a resolution < 10 °/h, a volume of a few tens of cm^3, and a weight < 1 Kg, which would represent a significant advance of the state of the art.

To experimentally verify the predicted performance, we are now designing the test bench to characterize our RMOG prototype under rotation. The electronic board to be included in the readout optoelectronic system has already been designed, fabricated, and tested.

Appendix

In this appendix, the expression (4) of the bias in the gyro output due to ΔI is derived. When $\Omega = 0$, the resonance frequency of the cavity is given by

$$\nu_0 = \frac{qc}{Ln_{\text{eff}}} \tag{A.1}$$

where q, which is an integer, is the resonance order, c is the speed of light in a vacuum, and L is the resonator length.

If the cavity is excited by two beams, they counterpropagate in the resonator with different velocities, which are equal to [28]:

$$\begin{aligned} v_{\text{CW}} &= \frac{c}{\sqrt{n_{\text{eff}}^2 + (n_2/A_{\text{eff}})(I_1 + 2I_2)}} \cong \frac{c}{n_{\text{eff}} + \frac{1}{2n_{\text{eff}}}(n_2/A_{\text{eff}})(2I_1 + I_2)} = \frac{c}{n_{\text{eff,CW}}} \\ v_{\text{CCW}} &= \frac{c}{\sqrt{n_{\text{eff}}^2 + (n_2/A_{\text{eff}})(2I_1 + I_2)}} \cong \frac{c}{n_{\text{eff}} + \frac{1}{2n_{\text{eff}}}(n_2/A_{\text{eff}})(I_1 + 2I_2)} = \frac{c}{n_{\text{eff,CCW}}} \end{aligned} \tag{A.2}$$

where I_1 is the intensity of the clockwise (CW) propagating beam and I_2 is the intensity of the counter-CW (CCW) propagating beam, and $n_{\text{eff,CW}}$ and $n_{\text{eff,CCW}}$ are the effective indices of the CW and CCW beams, respectively.

The difference between the resonance frequencies relevant to the beams is

$$\Delta\nu = \frac{qc}{Ln_{\text{eff}}^2}\left(n_{\text{eff,CW}} - n_{\text{eff,CCW}}\right) = \frac{qc}{Ln_{\text{eff}}^2}\left[\frac{1}{2n_{\text{eff}}}(n_2/A_{\text{eff}})\Delta I\right] = \nu_0\left[\frac{1}{2n_{\text{eff}}^2}(n_2/A_{\text{eff}})\Delta I\right]. \tag{A.3}$$

Since $\Delta\Omega = \Delta\nu/S$, we have

$$\Delta\Omega = \frac{\nu_0}{2n_{\text{eff}}^2}\frac{n_2}{A_{\text{eff}}}\frac{1}{S}\Delta I. \tag{A.4}$$

Acknowledgment

The sensor was modeled, designed and fabricated under the ESA IOLG project frame. The authors wish to thank ESA/ESTEC for providing the sensor.

References

[1] M. N. Armenise, C. Ciminelli, F. Dell'Olio, and V. M. N. Passaro, *Advances in Gyroscope Technologies*. Berlin, Germany: Springer-Verlag, 2010.
[2] C. Acar and A. Shkel, *MEMS Vibratory Gyroscopes*. Berlin, Germany: Springer-Verlag, 2009.
[3] C. Ciminelli, F. Dell'Olio, C. E. Campanella, and M. N. Armenise, "Photonic technologies for angular velocity sensing," *Adv. Opt. Photon.*, vol. 2, no. 3, pp. 370–404, Sep. 2010.
[4] W. Lawrence, "Thin film laser gyro," U.S. Patent 4 326 803, Apr. 27, 1982.
[5] O. Kenji, "Semiconductor ring laser gyro," JP Patent 60 148 185, Aug. 5, 1985.
[6] M. Armenise and P. J. R. Laybourn, "Design and simulation of a ring laser for miniaturised gyroscopes," in *Proc. SPIE*, 1998, vol. 3464, pp. 81–90.
[7] M. N. Armenise, M. Armenise, V. M. N. Passaro, and F. De Leonardis, "Integrated optical angular velocity sensor," EP Patent 1 219 926, Oct. 20, 2010.
[8] M. N. Armenise, V. M. N. Passaro, F. De Leonardis, and M. Armenise, "Modeling and design of a novel miniaturized integrated optical sensor for gyroscope applications," *J. Lightwave Technol.*, vol. 19, no. 10, pp. 1476–1494, Oct. 2001.
[9] M. Osinki, H. Cao, C. Liu, and P. G. Eliseev, "Monolithically integrated twin ring diode lasers for rotation sensing applications," *J. Cryst. Growth*, vol. 288, no. 1, pp. 144–147, Feb. 2006.
[10] S. Ezekiel and S. R. Balsamo, "Passive ring resonator laser gyroscope," *Appl. Phys. Lett.*, vol. 30, no. 9, pp. 478–480, May 1977.
[11] R. E. Meyer, S. Ezekiel, D. W. Stowe, and V. J. Tekippe, "Passive fiber-optic ring resonator for rotation sensing," *Opt. Lett.*, vol. 8, no. 12, pp. 644–646, Dec. 1983.
[12] K. Suzuki, K. Takiguchi, and K. Hotate, "Monolithically integrated resonator microoptic gyro on silica planar lightwave circuit," *J. Lightwave Technol.*, vol. 18, no. 1, pp. 66–72, Jan. 2000.
[13] G. Li, K. A. Winick, B. R. Youmans, and E. A. J. Vikjaer, "Design, fabrication and characterization of an integrated optic passive resonator for optical gyroscopes," in *Proc. 60th Annu. Meeting Inst. Navigation*, Dayton, OH, Jun. 7–9, 2004, pp. 211–216.
[14] C. Ciminelli, F. Peluso, and M. N. Armenise, "A new integrated optical angular velocity sensor," in *Proc. SPIE*, 2005, vol. 5728, pp. 93–100.
[15] G. A. Sanders, N. Demma, G. F. Rouse, and R. B. Smith, "Evaluation of polarization maintaining fiber resonator for rotation sensing applications," presented at the Optical Fiber Sensors, New Orleans, LA, 1998, paper FBB7, vol. 2 of 1988 OSA Technical Digest Series (Optical Society of America).
[16] M. Takahashi, S. Tai, and K. Kyuma, "Effect of reflections on the drift characteristics of a fiber-optic passive ring-resonator gyroscope," *J. Lightwave Technol.*, vol. 8, no. 5, pp. 811–816, May 1990.
[17] T. Imai, Y. Miki, S. Maeda, and K. Nishide, "Development of resonator fiber optic gyros," presented at the Optical Fiber Sensors, Sapporo, Japan, 1996, paper Ex2-1.
[18] Z. Jin, X. Yu, and H. Ma, "Resonator fiber optic gyro employing a semiconductor laser," *Appl. Opt.*, vol. 51, no. 15, pp. 2856–2864, May 2012.
[19] M. A. Terrel, M. J. F. Digonnet, and S. Fan, "Resonant fiber optic gyroscope using an air-core fiber," *J. Lightwave Technol.*, vol. 30, no. 7, pp. 931–937, Apr. 2012.
[20] H. Mao, H. Ma, and Z. Jin, "Polarization maintaining silica waveguide resonator optic gyro using double phase modulation technique," *Opt. Exp.*, vol. 19, no. 5, pp. 4632–4643, Feb. 2011.
[21] C. Ciminelli, F. Dell'Olio, C. E. Campanella, and M. N. Armenise, "Numerical and experimental investigation of an optical high-Q spiral resonator gyroscope," in *Proc. 14th Transparent Opt. Netw.*, Coventry, U.K., Jul. 2–5, 2012.
[22] C. Ciminelli, C. E. Campanella, F. Dell'Olio, V. M. N. Passaro, and M. N. Armenise, "A novel passive ring resonator gyroscope," in *Proc. DGaO/SIOF Joint Meeting*, Brescia, Italy, Jun. 2–5, 2009, p. 64.
[23] C. Ciminelli, F. Dell'Olio, C. E Campanella, and M. N. Armenise, "Innovative integrated-optic resonator for angular rate sensing: Design, fabrication and characterization," in *Sensors and Microsystems*, G. Neri, N. Donato, A. d'Amico, and C. Di Natale, Eds. Dordrecht, The Netherlands: Springer-Verlag, 2011, pp. 345–349.
[24] *ESA-IOLG project 1678/02/NL/PA*, ESA, Paris, France, Dec. 2008, Final Report.
[25] C. Ciminelli, V. M. N. Passaro, F. Dell'Olio, and M. N. Armenise, "Three-dimensional modelling of scattering loss in InGaAsP/InP and silica-on-silicon bent waveguides," *J. Eur. Opt. Soc.-Rapid Publ.*, vol. 4, pp. 09015-1–09015-6, 2009.
[26] K. Iwatsuki, K. Hotate, and M. Higashiguchi, "Eigenstate of polarization in a fiber ring resonator and its effect in an optical passive ring-resonator gyro," *Appl. Opt.*, vol. 25, no. 15, pp. 2606–2612, Apr. 1986.
[27] G. A. Sanders, M. G. Prentiss, and S. Ezekiel, "Passive ring resonator method for sensitive inertial rotation measurements in geophysics and relativity," *Opt. Lett.*, vol. 6, no. 11, pp. 569–571, Nov. 1981.
[28] W. W. Chow, J. Gea-Banacloche, L. M. Pedrotti, V. E. Sanders, W. Schleich, and M. O. Scully, "The ring laser gyro," *Rev. Mod. Phys.*, vol. 57, no. 1, pp. 61–104, Jan. 1985.